Analysis of the Rigid-Body Fluid-Structure Interaction on a Log Boom

Eduardo Tadashi **Katsuno**[b,a], Felipe Santos de **Castro**[b,*], João Lucas Dozzi **Dantas**[b,c]

[a] *University of Duisburg-Essen, Institute for Ship Technology and Ocean Engineering, Bismarckstr. 69, 47057 Duisburg, Germany*
[b] *Institute for Technological Research, Energy Infrastructure Laboratory, 532 Prof. Almeida Prado Ave., 05508-901, São Paulo, Brazil*
[c] *University of Strathclyde, Department of Naval Architecture, Ocean & Marine Engineering, 100 Montrose Street, G4 0LZ, Glasgow, United Kingdom*

Abstract

Log booms are modular and floating structures that partially cross the hydroelectric power plant reservoir to retain and deflect floating objects in the river that can damage and clog the turbine and reduce energy availability. In rivers with a high volume of logs or vegetation, the correct design of these structures is essential to ensure the operability of the hydroelectric power plant. In order to aid in the design of log booms, this paper proposes a method to predict the hydrodynamics forces and movement of log boom lines using CFD tools. Due to the high computational cost of simulating the entire line, simulations are conducted only on a single log boom module using boundary conditions that simulate the interference effects from its adjacent ones, considering different velocity magnitudes and direction combinations. The individual module results are composed to obtain the expected forces on the log boom line. A towing tank experiment with a model-scale model of a segment of the log boom line is conducted to verify the reliability of the numerical model results, comparing the module movement (heave and pitch) and line extremity tension forces. The agreement between numerical and experimental approaches shows that the proposed method can be used to predict the tension in the log boom line and evaluate other conditions, log boom geometries, or line shapes.
Keywords: Rigid-body FSI, CFD, Towing tank, Log boom, Hydroelectric power plant

---

*Corresponding author
Email addresses: eduardo.katsuno@uni-due.de (Eduardo Tadashi **Katsuno**), fscastro@ipt.br (Felipe Santos de **Castro**), joao.dantas@strath.ac.uk (João Lucas Dozzi **Dantas**)
URL: orcid.org/0000-0003-2818-3518 (Eduardo Tadashi **Katsuno**), orcid.org/0000-0002-9431-0506 (Felipe Santos de **Castro**), orcid.org/0000-0002-6482-0222 (João Lucas Dozzi **Dantas**)

This is a peer-reviewed, accepted author manuscript of the following article: Katsuno, E. T., Dantas, J. L. D., & de Castro, F. S. (2022). Analysis of the rigid-body fluid–structure interaction on a log boom. Journal of Fluids and Structures, 115, [103788]. https://doi.org/10.1016/j.jfluidstructs.2022.103788

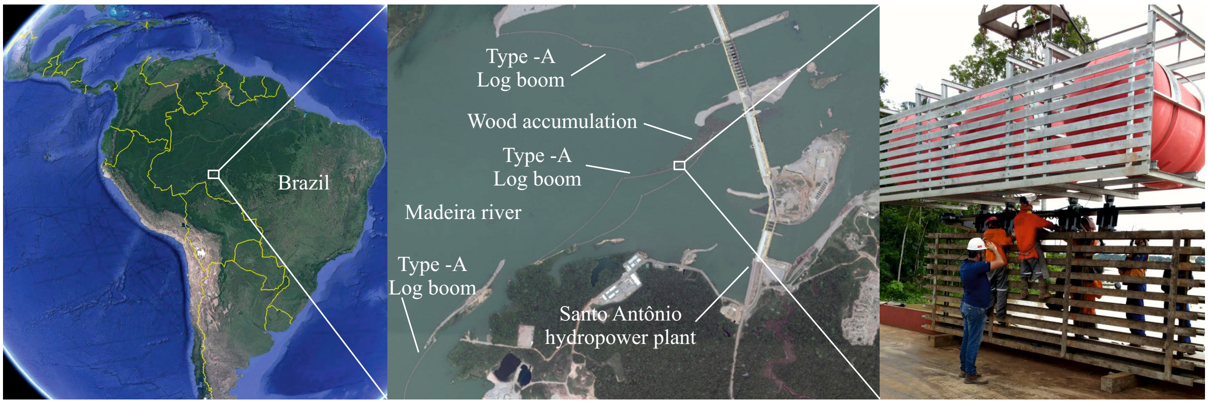

Figure 1: Location of Madeira River and the Santo Antônio hydropower plant (left); top view of the Madeira River, showing several log boom lines (center); and a log boom module (right). Source of left and center figures: Google Earth, map data: Google, Maxar Technologies, SIO, NOAA, U.S. Navy, NGA, GEBCO and Landsat/ Copernicus.

Nomenclature	
F_x, F_y	Axial and lateral forces (see Fig. 4)
C_x, C_y	Axial and lateral force coefficients (see Eq. (7))
Fr	Froude number, $Fr = v_a / \sqrt{g\,\ell}$
h_0	Log boom height at $\alpha = 0°$ (see Fig. 2)
v_a	Far-field flow velocity (see Fig. 4)
S_{ref}	Reference area (see Tab. 1)
α	Chassis' trim angle (see Fig. 2)
β	Side-slip angle (see Fig. 4)
ℓ	Characteristic length (see Tab. 1)

1. Introduction

As the demand for energy supply intensifies with the economy's progress, allied with sustainability, hydroelectricity plays a significant role in the world scenario. According to Girling et al. (2016), hydropower provides 71% of all renewable energy and has grown 39% from 2005 to 2015, mostly in emergent markets. Brazil is an example of this growth, corresponding to 8.6% of total global capacity, mainly due to the hydropower plant installations in the Amazon rainforest region in the last decades. The Madeira River is a major tributary of the Amazon River, having an extension of 3,315 km. It contemplates the Santo Antônio hydropower plant, Fig. 1, with a total installed power capacity of 3.5 GW, the fourth largest plant in Brazil.

The incidence of debris is an essential factor to consider when designing outlet works for dams, reservoirs, and in the design of navigation locks. The primary need for control is to prevent debris from obstructing water passage or damaging equipment such as turbines (Perham, 1987). In addition, floating debris induce clogging of spillway openings, decrease the reservoir's flood storage capability and induce more loading on the dam structure. The accumulation of debris may lead the water level upstream to rise, which could cause dam's overtopping and failures and should be considered in terms of safety aspects (Hassan, 2020). Debris booms arise as a solution to contain or deflect the undesired objects from reaching the turbines. They are generally applied on ice holding (Abdelnour, 2001; Morse, 2001), litter containment (Slat, 2014; Brambini et al., 2017), oil spill (Lo, 1996), or general river debris (Wahl, 1992). Santo Antônio dam is subject to a very demanding scenario: high flow rates that can reach up to $60\,000\,\mathrm{m^3/s}$, with some regions with velocities higher than $3\,\mathrm{m/s}$, combined with large quantities of logs transported in the river results in log-accumulation zones. Due to these characteristics, the Santo Antônio hydropower plant uses a custom log boom, a debris containment grid specially focused on containing and deflecting wood logs and other larger debris, as shown in Fig. 1.

In total, Santo Antônio hydropower plant uses eight different log boom lines, ranging from 70 m to almost 1 km, installed in their upstream basin. Due to the local river stream condition, these lines can be assembled using different log boom module types, depending on the necessity of higher buoyancy or structural strength. The log boom operation creates several fluid-structure engineering challenges, and therefore identifying the main aspects of its behavior is part of the improvement process.

The log boom module is a blunt body composed of grids made of structural beams and three floaters inside a cage. Presenting many sharp corners in its geometry, it causes several flow separation points, generating a highly complex flow characterized by high turbulence regions. Due to these characteristics, computational fluid dynamics (CFD) tools present a practical way to analyze the hydrodynamics of these structures, allowing simulations in several conditions and geometries that other methods cannot easily make. During the last years, the computational capability has become more powerful, allowing more complex simulations, which usually had to be simplified. The problem of rigid-body fluid-structure interaction (FSI) using CFD tools is present in several fields of study because of this advancement of computational power. Examples of rigid-body FSI studies can be found in studies of wave energy converters (Yu and Li, 2013; Gu et al., 2018), interactions of side-by-side vessel bodies and the fluid flow of the wave volume (Chua et al., 2018a,b), or in the study of floating offshore wind turbines (Leble and Barakos, 2016; Liu et al., 2017; Tran and Kim, 2018). The rigid-body FSI is studied in ship hydrodynamics (Terziev et al., 2018) due to the coupling among the sinkage, trim, and ship resistance coupled with the fluid flow. As presented in further sections, the current problem of the rigid-body FSI of the log boom module has some similarities with the ship hydrodynamics, as both are two-phase flows that consider the movements of sinkage, trim, and forces coupled with fluid flow.

Experimental hydrodynamic techniques applied to bodies with complex geometries have an application that can guide them toward their operation understanding. An interesting study was conducted by Ådnanes (2011) comparing four distinct methods to predict forces and deformations on a hanging fishing net cage. In one of the methods, net is assumed as a catenary curve and used previous lift and drag coefficients, from experimental data of tests performed by Løland (1991), to create a semi-empirical tool to calculate loads and deformation on nets in uniform current. Castro

(2021) has conducted an experimental investigation of log booms analyzed as truncated lines and individual bodies to predict their dynamic behavior in the presence of hydrodynamic flow with debris.

In recent works of Katsuno et al. (2017) and Castro et al. (2017b), the dynamic behavior and the hydrodynamic forces of the Santo Antônio's log boom module in different flow velocities and directions have been investigated numerically and experimentally. These results were used as a reference to verify the accuracy of simplified model results. Later, in Katsuno et al. (2018a) and Katsuno et al. (2018b), a simplified model of a log boom module using porous media has been developed, in order to check the feasibility of simulating the log boom line with simplified modules. However, a proper comparison of the log boom motion and the line extremities' forces was not yet been carried on.

A proper understating of the hydrodynamics of a log boom line is essential to avoid structural damages, which can compromise the efficiency and the availability of electricity from the hydropower plant. Conducting experiments with all employed log boom geometries in the Madeira River is unfeasible due to the limited availability of the towing tank. Furthermore, due to the width of towing tanks, it would be inconceivable to represent the actual condition of several log booms connected, needing to test a truncated form of the log boom line. Numerical methods are an option to analyze the hydrodynamics of several types of log booms, but the credibility of the results must be checked with experiments.

This paper proposes a method to simulate a log boom line behavior using numerical tools. As simulating the whole log boom line using CFD tool is computationally unfeasible, the method simulates only a single log boom module, considering the interference effects from its adjacent ones and obtaining the hydrodynamic forces. Results are used in a numerical model to compose and estimate the expected forces on the log boom line. In order to check both CFD method and the line model, the experimental campaign is conducted, where a model-scale truncated log boom line is tested in a towing tank. Two parts of validation are performed: the first is to compare the module motion, heave and pitch, obtained from CFD and experimental values from towing tank tests. Then, truncated log boom lines are assembled and tested with load cells to obtain the forces and compare the results with the log boom line method. This work focuses on the hydrodynamic effects of river flow on the log boom structure. In other words, this work does not consider the effect of wood accumulation.

This paper is organized as follows: in Sec. 2, the log boom is presented, with the geometry descriptions and weights. Section 3 presents the numerical method for the hydrodynamic analysis of the log boom module and the procedure to estimate the log boom line forces, while Sec. 4 presents the experimental methods, showing the facility to test the log boom line, instrumentation methods, and equipment. Section 5 presents the numerical results of the forces and motions of a single log boom module obtained via CFD. Then, Sec. 6 shows the first part of the results, comparing the heave and the pitch motion of a log boom module from numerical and experimental methods. Section 7 also compares the numerical and experimental methods to estimate the forces on the extremities of log boom line conditions. Finally, in Sec. 8, conclusions and future works are discussed.

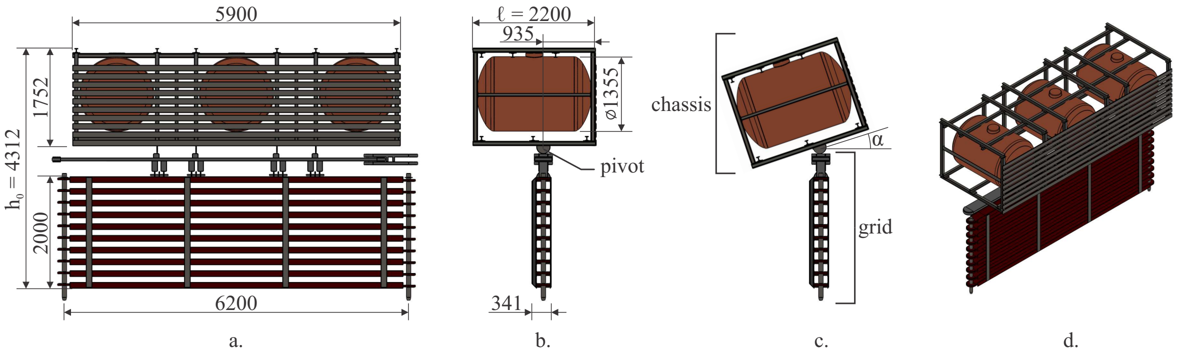

Figure 2: Main dimensions of type-A log boom (units in millimeter): a. Front view; b. Lateral view; c. Indication of chassis, grid and the trim angle α; d. Perspective view.

2. Test case - Santo Antônio's log boom description

Santo Antônio's log boom lines are floating grids connected side by side to protect the plant machinery against floating debris. Each unit is composed of three floats framed on a steel cage attached to a grid, as seen in Fig. 1. This modular structure is arranged continuously, creating a partially submerged line. Its extremities are anchored to concrete pillars embedded into the riverbed. It has been conceived to operate in very severe conditions, influenced by turbulence effects and the existence of vast amounts of debris.

Although several types of log boom are used in Santo Antônio, they are geometrically similar, changing some small characteristics, such as the pivot point, mass, or the number of beams. The test case is based on the type-A log boom module, used in the lines indicated in Fig. 1 and described in Fig. 2. Type-A is chosen because it is the most used model in Santo Antônio, and is also used in lines with the most significant loads. The upper part, called the chassis, connects to a longitudinal reinforced beam connected to a grid. The chassis weighs a total of 2,247 kg, whereas the lower part, the grid, weighs 2,861 kg. Two rods link the grids, while four pivots link the reinforced beam and chassis, all forming pin connections in which rotational movement is allowed but limited to 20°. The angle α is the trim angle between the chassis and the normal angle of the grid, as indicated in Fig. 2(c). Its lateral connection between modules consists of a steel coupler and shaft passing through the grid.

3. Numerical methods

The CFD approach has been developed to assess the hydrodynamics of a log boom. Its multi-body geometry, load characteristics, and motion behavior make it a complex problem to be addressed. The software Siemens Star-CCM+ version 13 double-precision, a cell-center finite volume method CFD, is used for all simulations, including the mesh generator and the post-processing tools. The geometries are represented using 3D CAD (Computer-Aided Design) software based on the project description and measurement of the log boom installed on the hydropower plant. The CAD drawing is also used to obtain the inertia properties of the bodies.

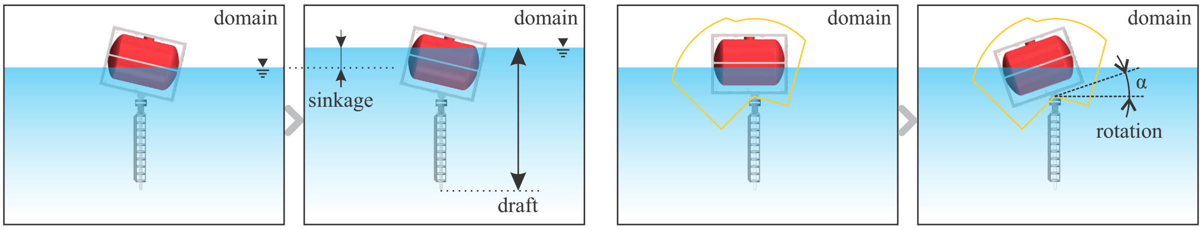

Figure 3: Two degrees of freedom (DoF) considered for numerical simulations: log boom module's heave (left) and pitch motion (right).

3.1. Numerical representation of a log boom module

The simulation of an entire log boom line would demand a high computational cost. Therefore, just one log boom module is simulated, with the sides having a periodic condition. This simplification is valid since the log boom module is almost symmetric, and the line is very long, 100 to 200 times the length of the module. Additionally, the angle between adjacent modules is small, considering that one side of a log boom has the same flow topology as the other side.

Regarding the movements of a log boom module, there are two important motions to be represented: the chassis rotation around the connection axis between the grid and chassis and the sinkage of the whole log boom module. For simplification purposes, they are treated from here now as the module's pitch and heave motion. Two regions are proposed to simulate these degrees of freedom (DoF): one that contains the domain and the grid, and another that contains the chassis. The overset approach is used to simulate the rotation, which is adequately explained in the following sections. For the heave movement, the wave line reference changes on the boundaries, simulating the water level changing. Figure 3 shows the numerical schematic to simulate the heave and pitch motion, as well as the definition of the draft.

The body motions are numerically calculated considering the bodies' hydrodynamics, inertia, gravity, and connections. The resultant force and moment acting on the body can be written as:

$$m\frac{d\mathbf{v}}{dt} = f_r\left(m\mathbf{g} + \sum_f p_f \mathbf{a_f} - \sum_f \boldsymbol{\tau}_f ||\mathbf{a_f}||\right) + \mathbf{f_c}, \quad (1)$$

$$\mathbf{M}\frac{d\boldsymbol{\omega}}{dt} + \boldsymbol{\omega} \times \mathbf{M}\boldsymbol{\omega} = f_r\left[\sum_f \left[\mathbf{r_f} \times \left(p_f \mathbf{a_f}\right)\right] - \sum_f \left[\mathbf{r_f} \times \left(\boldsymbol{\tau}_f ||\mathbf{a_f}||\right)\right]\right] + \mathbf{q_c}, \quad (2)$$

in which m is the mass of the body; $\mathbf{v}$, velocity of the center of mass; f_r, time-ramping function (from 0 to 1); $\mathbf{g}$, gravity; $\sum_f$, sum on all element faces on the body; p_f, pressure at face f; $\mathbf{a_f}$, area vector of face f; $\boldsymbol{\tau}_f$, shear stress acting on face f; $\mathbf{f_c}$, external forces due to body connection; $\mathbf{M}$, tensor of the moments of inertia; $\boldsymbol{\omega}$, angular velocity of the rigid body; $\mathbf{r_f}$, distance vector from the body center of mass to the center of face f; and $\mathbf{q_c}$, external moments due to body connection.

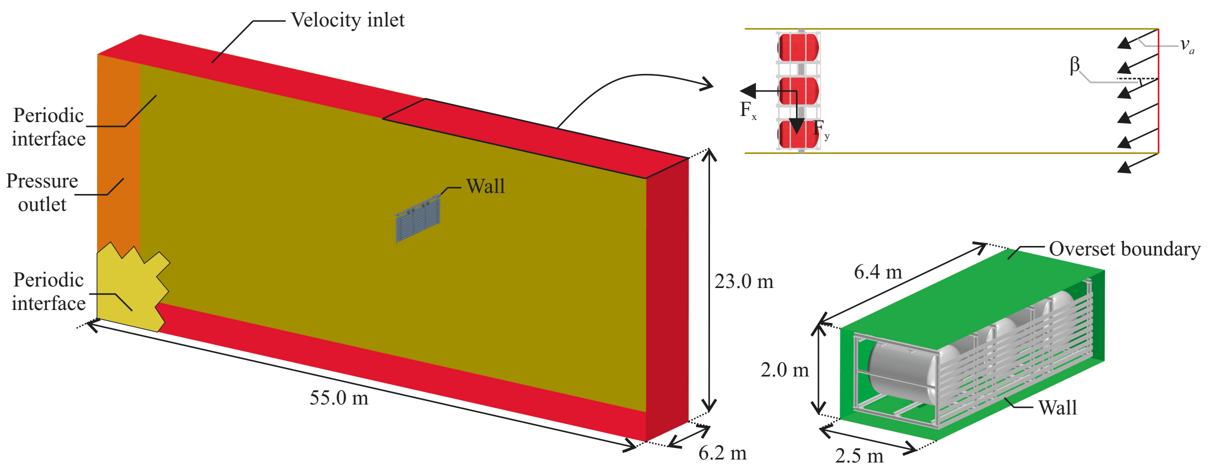

Figure 4: Geometry dimensions and the adopted boundary conditions for the domain region (left); top view, indicating the velocity v_a and side-slipe angle β of velocity inlet boundary condition (top right); and the chassis region (bottom right).

3.2. Domain geometry and boundary conditions

The dimensions of each region and the boundary conditions are shown in Fig. 4. The width of the domain corresponds to the width of one log boom module. The overset boundary covers the chassis region, which interpolates with the main domain mesh.

The numerical treatment for velocity inlet boundary conditions is that velocity, turbulence kinetic energy, and specific dissipation are specified while the pressure gradient is zero. The velocity is defined by the magnitude of the far-field flow velocity v_a and the side-slip angle β, as shown schematically in Fig. 4. This way, it can simulate the log boom module at an inclined water flow condition. For pressure outlet boundary conditions, velocity, turbulent kinetic energy, and specific dissipation gradients are zero, while the pressure is defined. The flat wave model defines the volume of fractions, discussed in the following subsections.

3.3. Mesh topology

In both regions, hexahedral mesh topology is used. In the domain region, volume controls for mesh refinement are made in regions close to the log boom, decreasing the density of elements according to the wake distance. Also, the elements are refined in the waterline region to represent the water-air interface better. Volume control is used to refine the mesh within the possible trajectories of chassis rotation, maintaining the same element size to perform the overset interpolation.

The refining volumes, domain, and chassis meshes are presented in Fig. 5. Elements have sizes similar to the overset refine zone on the domain region, as a recommendation of Siemens (2018) to interpolate these two meshes to generate an equivalent unified mesh. It is considered that regions outside the chassis use the domain mesh; overlap regions use the chassis mesh; and at the edge, an intermediate cell zone belonging to two regions. An essential

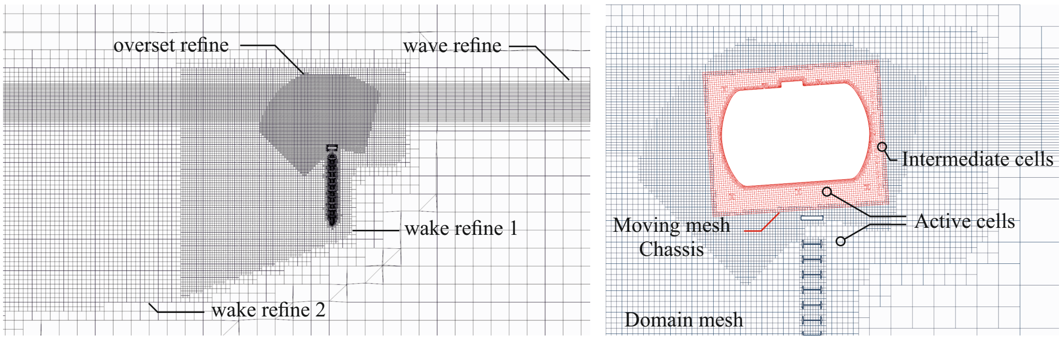

Figure 5: Mesh topology of the domain region (left) and after the hole-cutting between domain and chassis meshes (right).

advantage of this method is that the mesh is interpolated at each time-step, representing the chassis' rotation without remeshing.

3.4. Numerical setup

The unsteady Reynolds-averaged Navier-Stokes (uRANS) equations are used to model the flow field. The Volume of Fluid (VoF) Eulerian multiphase model is used to represent the phase mixture. Water and air are considered incompressible, and its densities are set as $997.6\,\mathrm{kg/m^3}$ and $1.184\,\mathrm{kg/m^3}$, respectively; and the dynamic viscosities, 8.887×10^{-4} Pa s and 1.855×10^{-5} Pa s, respectively. The $k - \omega$ SST model (Menter et al., 2003), is adopted. The flat wave model is adopted to define the multiphase conditions, using numerical damping in inlet and outlet boundary conditions to minimize the effect of wave reflection and ensure a better convergence. The wave damping is done by adding a term of resistance in the z-momentum (direction of gravity) of the Navier-Stokes equations, following the method proposed by Choi and Yoon (2009). Turbulence intensity is set as 10%, based on the mean value of turbulence intensity found in rivers (McQuivey, 1973).

The Courant number is maintained the same throughout the simulations, defining the timestep as a function of the mean element size and the far-field flow velocity, varying between 6.1×10^{-5} s and 9.0×10^{-5} s. The volume-average Courant number is around 0.02 - 0.03. At the beginning of simulations, heave and pitch are frozen due to fluid stabilization. Then, the movements are gradually released and awaited to stabilize. Finally, the time step is decreased, some more iterations are run, then the results are collected.

The simulations ran up to the physical time between 50 s and 250 s, depending on the monitoring of the forces to achieve a constant value or a constant-oscillatory behavior with a constant mean value. Then, the mean value of the last 1,500 time-steps is assumed as the considered output.

3.5. Catenary model

Looking closely at Fig. 1, it is possible to note that the log boom lines assume shapes on the water surface that resemble hanging cables. However, their form comes from the interaction with water and debris instead of their weight.

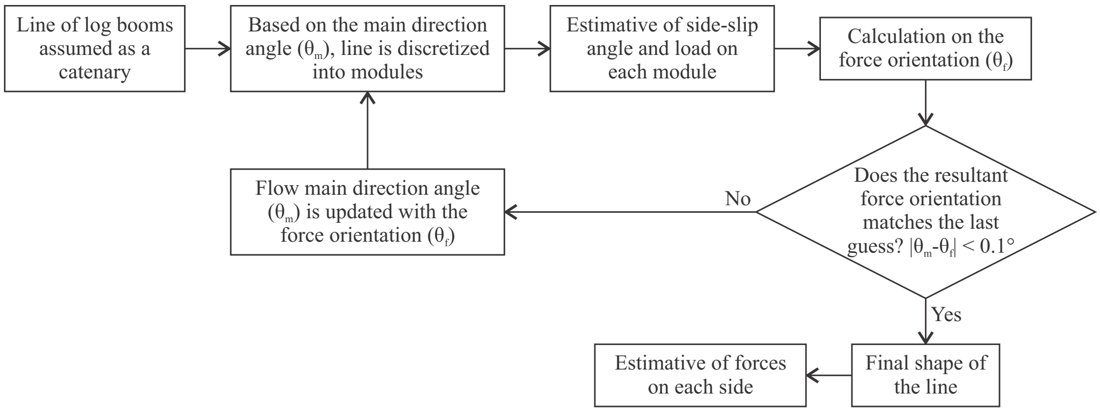

Figure 6: Flowchart of the numerical estimative of loads on a log boom line.

Any chain or cable, neglecting its flexural rigidity, supported at its ends and hanging under its weight, when static balanced, assumes a curve shape called catenary (Papini, 2010). Assuming that the line presents a unidirectional force along its length and each module is connected by a revolute joint, not transferring moment, the geometry can be represented by an asymmetrical catenary as a first estimative. Considering the catenary curve positioned on a Cartesian coordinate system, between the endpoints (x_0,y_0) and (x_1,y_1). In the catenary formulation, it is possible to determine its format equation if the extremities coordinates and length L are known as follows:

$$y(x) = a \cosh\left(\frac{x - x_{\min}}{a}\right) + b, \tag{3}$$

in which the parameters a, $x_{\min}$, and b are expressed as:

$$\sqrt{L^2 - (y_1 - y_0)^2} = 2\,a\,\sin\left(\frac{x_1 - x_0}{2\,a}\right) \tag{4}$$

$$x_{\min} = x_0 - \frac{1}{2}\left[a\,\ln\left(\frac{L + y_1 - y_0}{L - y_1 + y_0}\right) - (x_1 - x_0)\right] \tag{5}$$

$$b = y_0 - a\cosh\left(\frac{x_0 - x_{\min}}{a}\right) \tag{6}$$

The coordinates of the extremities and the length of each module, therefore the entire line, are known. As a first guess, the line is assumed to have the main direction of the load (θ_m) parallel to the flow direction during experiments. Based on the CFD results, the side-slip angle of each log boom and the force on each element are calculated. In order to better estimate the shape of the line, the resultant force's orientation (θ_f) of the entire line is compared with the first estimative, and, in case of difference, θ_f is assumed as the main direction. Then, the shape of the line and forces are recalculated altogether. A flowchart of the process to estimate the shape of the line and calculation of forces is presented in Fig. 6.

Figure 7: IPT's Towing Tank.

4. Experimental methods

The experimental campaign was carried out at the Towing Tank of the Institute for Technological Research (IPT) in São Paulo, Brazil. The basin is 280 m long, 6.6 m wide, and 4 m deep, shown in Fig. 7. Tests were focused on measuring the loads at the ends of a segmented line of log booms and the motion of two modules, varying the line geometry and velocity magnitude.

The tests used a 1:10 scale model, which presented the best agreement among the number of modules, dimensions of the towing basin, quality of measurement, and viability of the experimental matrix. The log boom hydrodynamics is assumed to be dominated by inertial and gravitational effects (i.e., surface-flow problem), being reasonable to use the Froude similarity to transform the river stream velocity measured at Santo Antônio's dam to the towing speed in the experiments. The scale effect related to the Reynolds number was not corrected, as it was assumed to have a low dependency on viscosity/friction effects, being negligible. This assumption relies upon the log boom design characteristics: the geometry is composed of several structures with sharp edges, which results in several flows detachment points that do not change significantly with flow velocity; and the log boom does not have a large continuous surface that can develop the boundary layer (Bak Khoshnevis et al., 2015). The chassis length along the longitudinal axis was considered the characteristic length ℓ (see Fig. 2) for the Froude number calculation.

The reduced model was designed to reproduce most of its geometric details. All the metallic parts in the prototype are constructed using polycarbonate sheets, which provided enough structural resistance for the model to be handled and used in the tests. Except for the thickness, which was adapted to have a minimum of 1 mm, all dimensions were fully represented in the scale model. Floaters were built using PVC (polyvinyl chloride) pipes and ABS (acrylonitrile butadiene styrene) plastic. Considering the weight difference between real and scale log booms, some lead pieces were placed at the top of the chassis and in the grid beams as ballasts to ensure the hydrostatic similarity between them (see the right-hand side of Fig. 7). The main particulars of the real size and model scale are presented in Tab. 1. Mass values present some differences since the thickness of the elements were not fully represented in the model-scale

Table 1: Log boom module main dimensions.

Module	Height h_0 [m]	Characteristic length ℓ [m]	Width [m]	Mass [kg]	Reference area S_{ref} [m^2]
Real size	4.31	2.2	6.2	5,108	22.7
1:10 model-scale	0.431	0.22	0.62	5.296	0.227

module.

The instrumentation measures two quantities: loads acting at the ends of the truncated model and movements of some modules. For force measurement, eight S-Type S9M uniaxial load cells produced by HBM are used in each extremity of the line to measure the distribution of load among them. As in the full-scale prototype, the chassis has no structural function, and because of that, only the reinforced beam and grid were connected to the load cells through a set of tie rods. Tie rod models, used to anchor the log booms at the columns at the river, are also included in the final layout.

The motion was measured using four infrared cameras, Qualisys model Oqus 500, and spherical reflexive targets. External rods are installed to place the targets to allow the measurements on two modules, preventing them from getting wet. Figure 8 shows the final overview of the log boom model. The number of instrumented modules is defined based on the camera's visual range and their overlapping while measuring. The motion tracking apparatus measured the targets' position and the body's motion defined by them in a coordinate system that is fixed to the towing carriage and set during calibration steps.

The experiments consisted in towing the truncated model on two configurations that represent relevant conditions seen in the actual log boom lines: the symmetrical case, using five modules, represents the log boom regions in the most critical conditions, with higher loads and vertical movement due to the low sideslip angle; and the asymmetrical case, using seven modules, simulates the regions of the log boom used to facilitate the debris' flow along the log boom line, resulting in different loads and sinkage at each end. Figure 8 presents a top view of the test's schematics for the configuration with five modules, showing the line arrangement and the instrumentation devices' locations. Motion measurements are performed on the central log boom. Side plates were placed to minimize the hydrodynamic effects caused by the anchorage structure on the line model.

5. Numerical results of the log boom module

Simulations with six Froude number (from $Fr = 0.216$ to $Fr = 0.754$) and six side-slip angles ($\beta = 0°$ to $\beta = 75°$) are conducted, in total of 36 cases. Due to geometric limitations, the rotation of chassis is modeled if its value does not surpass 40°; otherwise, this angle is set to 40° and the rotation DoF is deactivated.

Figure 9 shows the CFD results in terms of non-dimensional outputs: trim angle α and draft ratio, which is the draft divided by h_0, the log boom height at $\alpha = 0°$ (see Fig. 2). Results are obtained from the last 1,500 iterations of the simulations, which is equivalent to the equilibrium condition. In cases of $Fr \geq 0.539$ and no side-slip angle, the

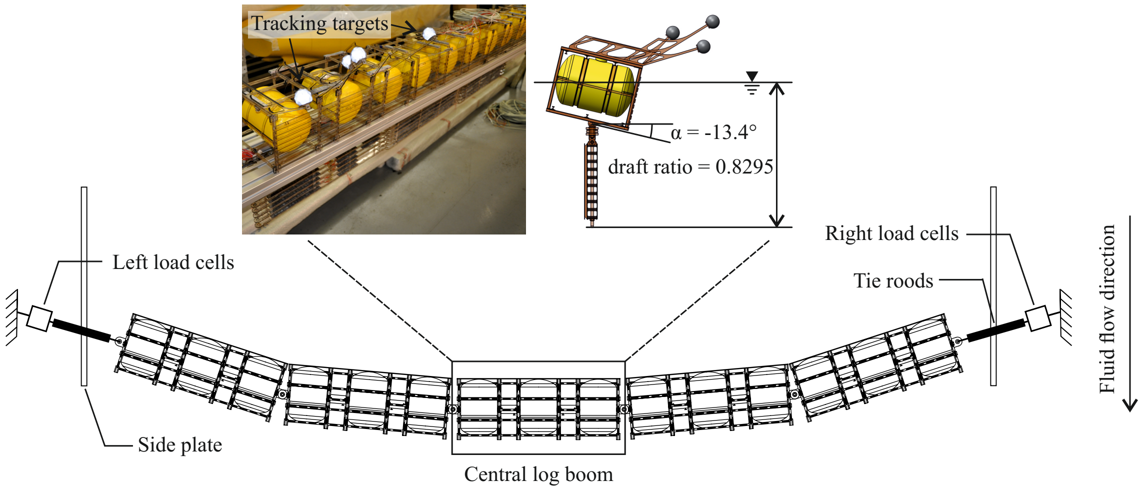

Figure 8: Towing tank test schematics, showing in detail the tracking targets and the static condition.

numerical model indicated a submerged log boom in a theoretical scenario of no external interference or influence from the rest of the line. Increasing the side-slip angle reduces the module draft ratio in all simulated cases. This effect is more significant for higher Froude numbers, especially when the numerical model indicates the submersion without a side-slip angle, meaning that the submerged modules can emerge not only by reducing the velocity but also by increasing the side-slip angle as coupled phenomena. The module's rotation results indicate that the trim angle increases with the Froude number and acts inversely proportional to the side-slip, similar to the observed in the draft ratio curve. This coupled motion indicates that higher side-slip angles should be adopted for the real line of log booms to attain better results in terms of floating debris retainment.

Figure 10 shows the longitudinal velocity, v_x, divided by the far-field flow velocity, v_a, in the mid-plane of the module to analyze the local fluid topology. In all these figures, the flow is in the perpendicular direction to the face of the chassis, i.e., the module has zero side-slip angle ($\beta = 0°$). It is observed that the chassis rotation angle increases as the speed increases. Higher speeds show a complete module sinkage for Fr above 0.539. A negative velocity region is observed at the bottom of the grid, indicating a high recirculation zone. For lower Fr, the magnitude of this effect is not intense, so the total hydrodynamic force pushes the grid up due to the log boom buoyancy. As the Fr increases, this phenomenon becomes more severe than the buoyancy, pushing down the log boom. As the log boom sinks, the buoyancy force from the floaters increases, balancing the forces in the vertical direction. When the log boom is fully submerged, the buoyancy force becomes constant, and the total hydrodynamic forces push down the log boom, explaining the high draft ratio results in Fig. 9.

6. Results: analysis of pitch and heave motion

This section studies the log boom movements using numerical and experimental methods to compare the heave and pitch values for different Froude numbers. The motion study analyzes the module's stability in each condition,

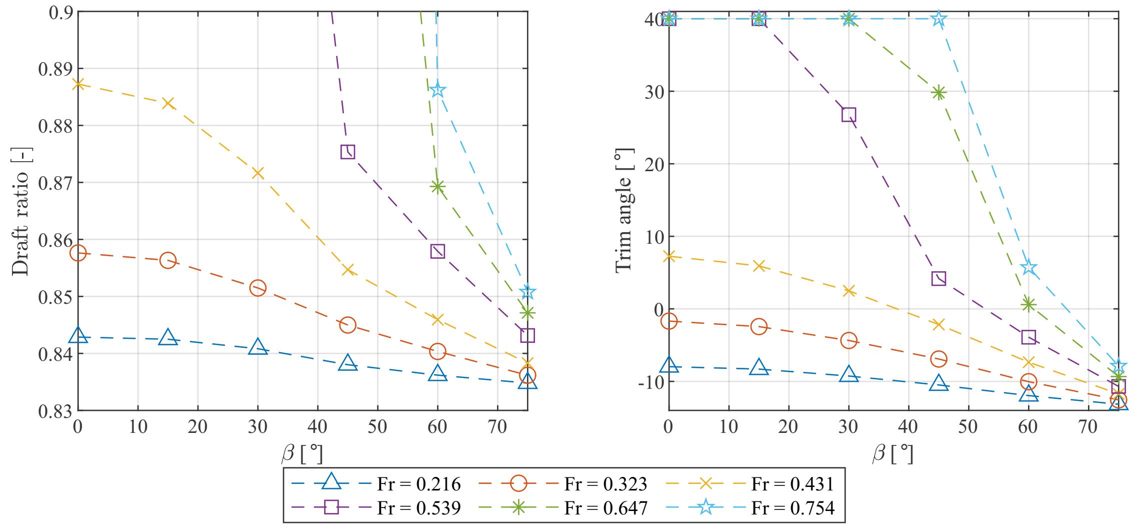

Figure 9: Draft ratio (draft divided by log boom height h_0) (left) and trim angle α (right).

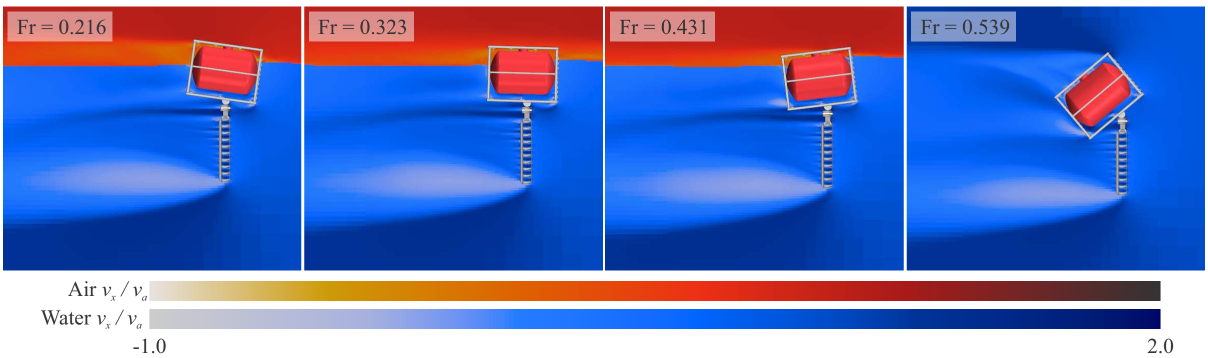

Figure 10: Velocity magnitude field distribution for 4 different Froude number conditions and $\beta = 0°$.

verifying if hydrodynamic loads can induce rotation and sinkage levels significant enough to reduce the log retention capability.

Results from Sec. 5 have shown that perpendicular flows, $\beta = 0°$, are the most critical conditions, presenting the largest amplitude of movements. Both movements significantly reduce as the side-slip angles increase, indicating that the side-slip angle attenuates the module movements. Thus, it is chosen this condition of side-slip angle $\beta = 0°$, using the motion measurements from the central log boom module in the tests with the symmetrical catenary condition, as seen in Fig. 8. It is important to notice that the simulations are carried out on the full-scale while the experiments, on a 1:10 model-scale, resulting in different far-field velocities. However, as the experiments are designed considering the Froude similarity, wave and pressure hydrodynamic forces should present similar behavior in both scales. Although the friction-related forces are not scaled correctly, requiring adopting a Reynolds similarity (which is unfeasible to achieve as the Froude similarity has been reached), it is expected that these forces are considerably lower than the pressure and gravity-related forces since the log boom geometry has several sharp corners, which induces flow separation and makes pressure forces more dominant than the shear ones.

Figure 11 shows the agreement between results obtained by CFD and experiments in terms of non-dimensional outputs: trim angle α and draft ratio. As shown in Fig. 8, the log boom module has a trim angle of 13.4° and a draft ratio of 0.83 at the hydrostatic condition ($Fr = v_a = 0$). Numerical values are obtained after the simulations reach a stationary condition, observing the simulations' iterative and temporal convergence. Experimental results are calculated by taking the mean value of 30 s to 60 s of acquired data, depending on the test speed, and observing the experiment to reach a stationary condition. It is interesting to notice consistency regardless of the different scale sizes on both approaches. Visual perception of the motion is presented in Figure 12, showing the experimental campaign in four Fr along with the equivalent numerical simulation, in which the analyzed module is highlighted. As the velocity increases, the pressure on the frontal face of the chassis increases, causing the rotation of the modules and, along with the grid's hydrodynamics, their sinking.

The results show good similarities between values predicted by the numerical model and those obtained by the pitch and heave analysis experiments. It is observed that increasing the Froude number increases the trim angle and draft ratio of the log boom module, becoming fully submerged at $Fr > 0.431$. The experimental apparatus has a limitation, given its attachment ends of the line that prevents the module from sinking and rotating further, which is seen by the slight difference that starts to appear at the highest Fr, compared to the numerical approach. Since the log boom application implies retaining floating debris, mainly at the water surface, its functionality becomes compromised at high Fr scenarios. The comparative results reinforce that the adopted CFD model is satisfactory for modeling the main movements of the log boom module. Furthermore, the comparison of model and full-scale shows to be a reasonable approach to compare movements on different body scales.

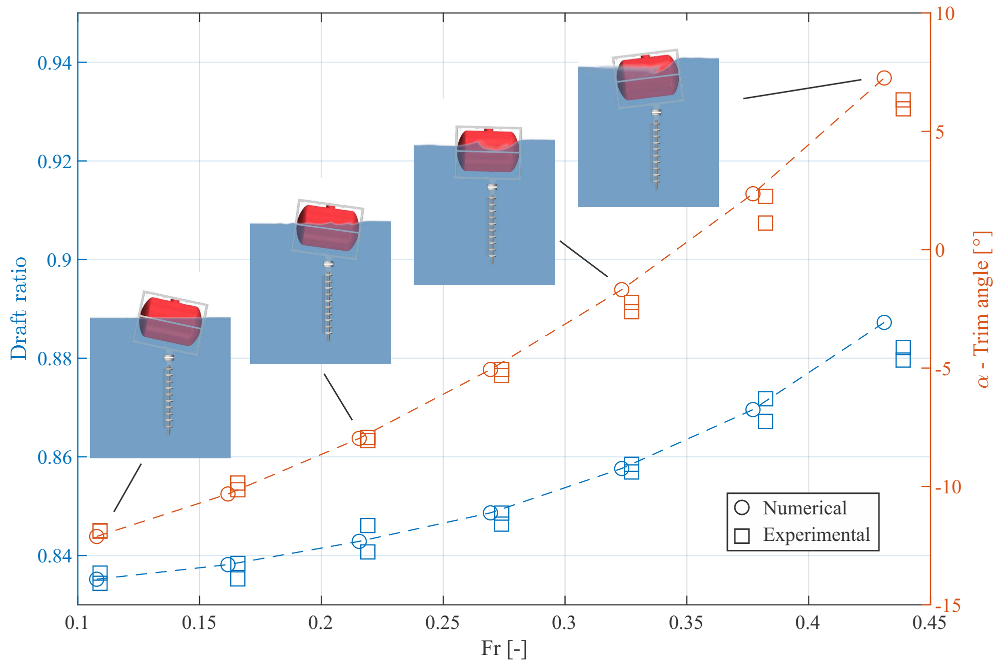

Figure 11: Numerical and experimental comparison of the draft ratio (draft divided by h_0) and trim angle α.

7. Results: force analysis in the truncated log boom line

Simulating the log boom line is a more complex problem than the module alone because the line is composed of several modules, each presenting its degree of freedom, which requires more computation power to be solved. An alternative solution is proposed: use the hydrodynamic results of the log boom module obtained in Sec. 5; interpolate these values to get an expression of expected forces as a function of the Froude number and side-slip angle; and, using a catenary-like model, sum the force contribution of each module to estimate the forces on the line extremities. A truncated model of the log boom line is adopted to validate this approach with experiments due to the width of the IPT's Towing Tank, as it would be inconceivable to conduct experimental campaigns with the scaled length of the log boom line because it would require significantly small modules, compromising the quality of measurements.

7.1. Interpolation of the force results

Figure 13 shows the axial and lateral force coefficients (i.e., in the body coordinate system, see Fig. 4) of the full-scale log boom module as a function of the side-slip angle. The dimensionless coefficients are used to transpose the results obtained in the full-scale numerical model into the expected forces on the experimental scale. These coefficients are defined as:

$$F_{x,y} = \frac{1}{2}\rho\, v_a^2\, S_{\text{ref}}\, C_{x,y}. \tag{7}$$

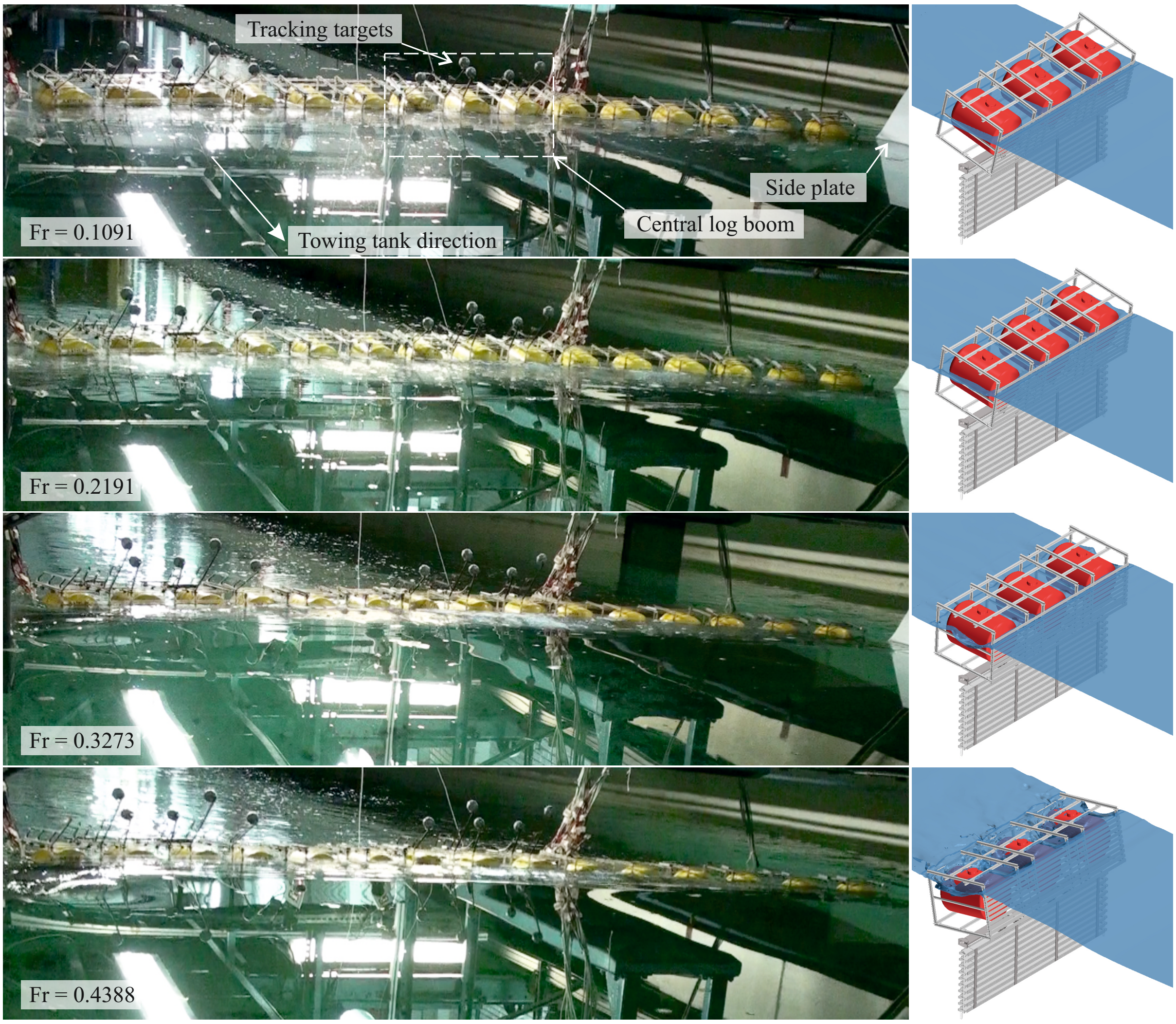

Figure 12: Model-scale experimental tests to measure the log boom motions conducted at IPT's towing tank (left) and the numerical results of full-scale log boom motions (right).

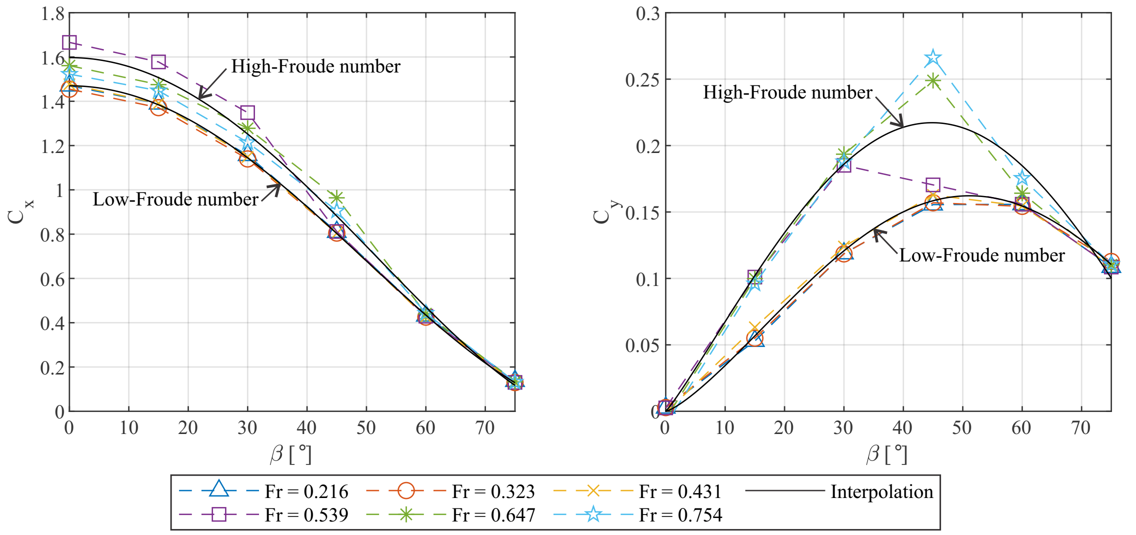

Figure 13: Axial (left) and lateral (right) force coefficients and proposed interpolating functions for low and high Froude conditions.

The results indicate that these forces have sine-cosine behavior regarding the side-slip angle. The coefficients seem to converge to the same curve for the group of $Fr = 0.216$ - 0.431, while higher Froude numbers ($Fr = 0.539$ – 0.754) seem to converge to a different curve, suggesting that the module sinkage has a significant effect on the axial and lateral force coefficients. In this way, two interpolations are proposed, matching the results of these two groups of Froude numbers. These coefficients are interpolated using a sine and cosine formulation, represented as:

$$\begin{aligned} C_x &= k_1 \left[\cos\left(k_2 \beta\right)\right]^{k_3}, \\ C_y &= k_4 \left[\sin\left(k_5 \beta\right)\right]^{k_6}, \end{aligned} \tag{8}$$

in which k_1, ..., k_6 are coefficients of the interpolation, defined by the least squares method based on the results shown in Fig 13. As it is required to have two curves of interpolation to accommodate the Froude number range, these two curves are merged by a blending function γ, using a hyperbolic tangent to blend these two curves of interpolation smoothly.

$$\begin{aligned} C_x &= \gamma \cdot 1.5973 \left[\cos\left(1.0714 \cdot \beta\right)\right]^{1.4637} + (1-\gamma) \cdot 1.4699 \cdot \left[\cos\left(1.0210 \cdot \beta\right)\right]^{1.6647}, \\ C_y &= \gamma \cdot 0.2172 \left[\sin\left(2.0065 \cdot \beta\right)\right]^{1.0933} + (1-\gamma) \cdot 0.1622 \cdot \left[\sin\left(1.7597 \cdot \beta\right)\right]^{1.2955}, \\ \gamma &= \frac{\tanh\left(42.7 Fr - 20.7\right) + 1}{2}. \end{aligned} \tag{9}$$

The C_x and C_y equations are designed to be easily used to integrate the force along the log boom line, as they are defined as a function of the local streamflow velocity and incidence.

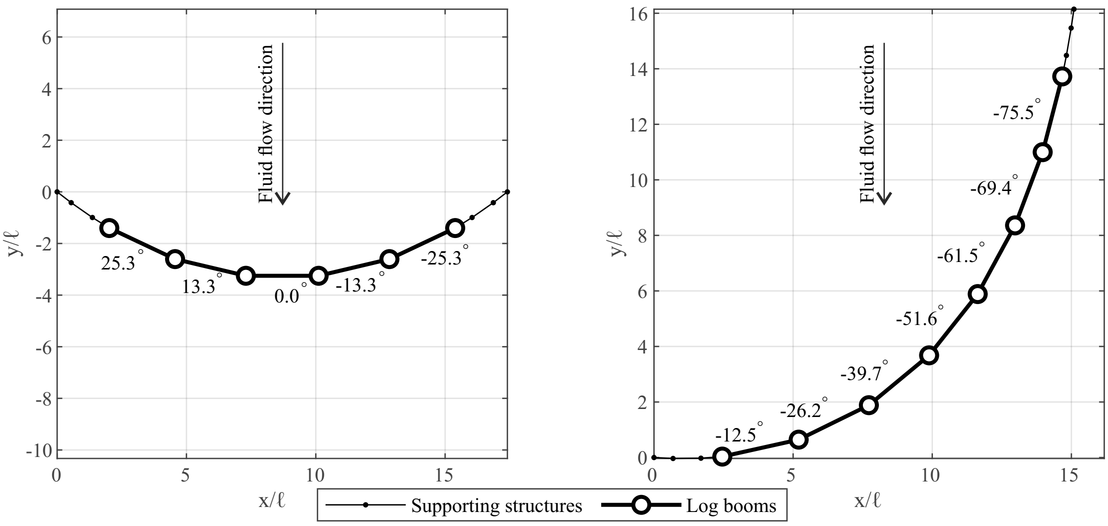

Figure 14: Log bom line shapes and positions for five (left) and seven modules (right).

7.2. Comparison of truncated log boom lines

The two truncated log boom lines presented in Sec. 4 are used to compare the numerical and experimental approaches. The symmetrical condition, with five modules, represents the regions with lower side-slip angles (higher loads). The asymmetrical condition (seven modules) depicts the cases with an increasing side-slip angle to facilitate the log flow. The module position and rotation are defined by the catenary model presented in Sec. 3.5. Figure 14 shows the log boom line shapes, in which the thicker solid lines represent the modules, while the thin ones describe the tie rods and load cells at the line ends. The circles represent the location of lateral pivot axes between log booms.

Figure 15 shows the results of the five modules log boom line for 11 different Froude numbers. Due to shape symmetry, the numerical results present the same values of left and right forces. The uncertainties are composed of the standard deviation of each measurement data set and are shown on a 95% confidence interval. Although the tests showed a slight difference between the left and right sides, due to some asymmetries and limitations of the joint elements to allow a proper curvature to the line, both sides are very close to the results obtained by the numerical model. The reasonable similarity of numerical and experimental results is also associated with the line's geometry, which presents low side-slip angles, resulting in significant contributions from the axial force C_x, instead of the lateral one C_y. Additionally, the minor variations of β angles result in similar force distribution along the line, making it closer to a fundamental formulation of a catenary. For high Froude numbers, experimental values have higher magnitudes than predicted by the numerical method. This behavior is attributed to (i): the expected sinking of the line at high Froude numbers (see the draft ratio of Fig. 9) generates vertical forces beyond the lateral and axial directions that are measured by the load cells and added up to the total force of the line; and (ii): the limitations of the chassis movement when dealing with high Froude numbers, which, as discussed previously, were adopted two interpolation curves to

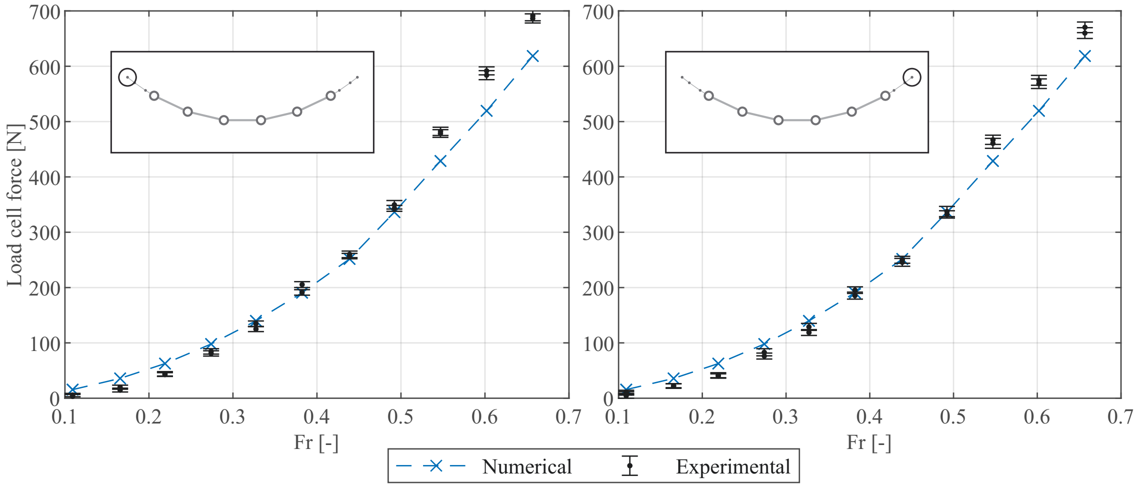

Figure 15: Numerical and experimental force comparison on the left and right extremities of a five-module log boom line.

separate the low and high-Froude cases.

Figure 16 shows the case with seven modules. As expected by the catenary formulation, the left load cell forces are lower than the right ones for numerical and experimental methods. This result is expected because of the shape of the log boom line, which presents greater load values at the upstream end to reach the equilibrium of forces in transversal and longitudinal directions. Comparing the experimental and numerical values, the forces on the right side present a good agreement between methods, with some differences on low Froude numbers ($Fr = 0.28$, for example). This difference is attributed to the friction between each module: due to the low advance velocity of the towing carriage, the catenary was not fully tensioned, leading the line to assume a compression behavior at the downstream end, indicated by the negative values at this Fr range. Moreover, as the tension on the right side is higher than on the left side, the friction effect is more significant for the left side for low Fr. After increasing the velocity, the truncated line becomes more tensioned, leading to the expected catenary shape.

Similar to the five-module case, the more significant difference between numerical and experimental in the left load cell force can also be attributed to the added sinkage force measured during the experiments. This additional force is measured by the load cells. They restrict the log boom vertical sinking movement in higher Froude numbers but are not predicted by the numerical method, as this restriction is not considered in the model. This supposition is reinforced by the right side, which presents a very good agreement between experimental measurements and numerical predictions. Therefore, it can be assumed that even for this case, which presents an asymmetric shape of a log boom line with high side-slip angles, the numerical estimative shows appropriate similarity compared with the experimental ones.

The study with 5 and 7 modules ensures that the numerical and experimental models have produced valuable results. Although some differences between approaches were observed, the results suggest that the proposed numerical

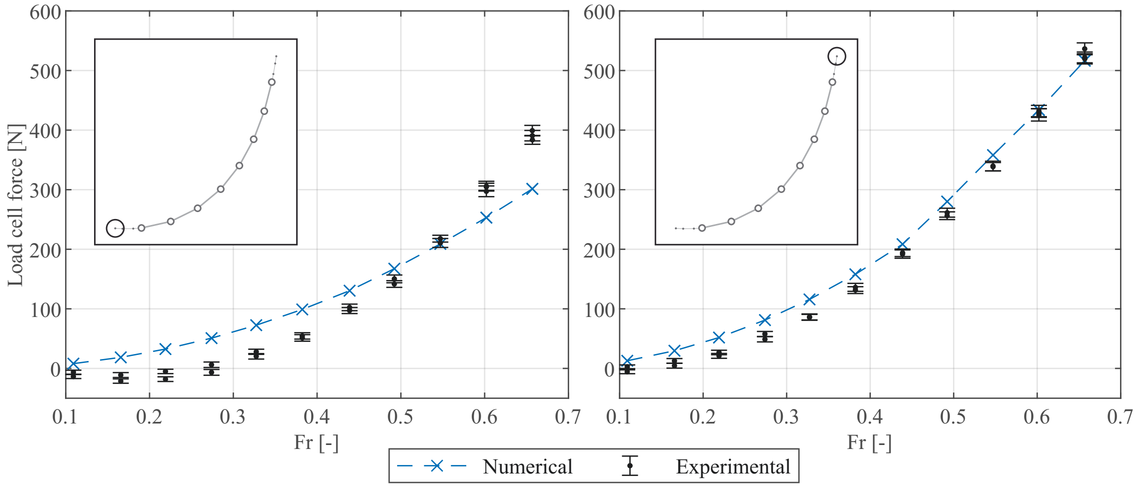

Figure 16: Numerical and experimental force comparison on the left and right extremities of a seven-module log boom line.

model developed to simulate the log boom line is satisfactory for predicting motion and forces. This factor contributes to the simplification adopted in the CFD model: simulating only one module and using periodic boundary conditions. The differences in forces at both ends caused by the inclination of the log boom line, also discussed in Castro (2021), are reproduced on both models. The differences in scales show that treating the variables in non-dimensional coefficients is justifiable to reproduce the FSI phenomenon at the adopted Fr range. The obtained coefficients can be considered for estimating forces on a complete log boom line.

For the application in the Madeira river, some observation needs to be addressed:

- The large width of the Madeira river makes the streamflow velocity different along an extended log boom line, which yields different forces in each module. A catenary shape may not be ideal for estimating the log boom line. To improve the prediction, a truss-based finite element method model should be a good approach to estimate the line shape and the load distribution (Chreim et al., 2018).

- As observed in Fig. 15 and 16, high Froude number conditions can increase the log boom line forces and promote the sinkage of modules. Special care should be taken on these conditions, as the log boom movement reduces its retention capacity and demands high loads, compromising its structural integrity, especially at the fixing points, i.e., extremities of the line.

- Considering the real case, the arrangement of the log boom lines should prioritize greater side-slip angles, as this condition results in lower forces and sinkage along the line, and the overall arrangement facilitates the logs to flow away from the log boom, i.e., less retained logs. However, this is not feasible for all log boom lines in Santo Antônio, as the river flow topology is disrupted by the turbine intakes, resulting in a more aligned flow close to the dam.

- The proposed method was also applied for the other types of log boom modules in the dam, with different coefficients of interpolation, k_1, ..., k_6 from Eq. (7). It was noticed that modules with higher frontal area, larger grids or floaters, and higher weight-buoyancy ratio (structures with high density) generate greater hydrodynamic forces.

- It is important to note that the presented method does not take the vertical force distribution along the module. As presented in Castro et al. (2017a), depending on the tested condition, the load stress can concentrate in the bottom or top part of the module, resulting in elements with higher stress than others.

The method presented in this work can be extended to other floating barriers composed of several modules wherein the length of the line is considerably greater than its height. The booms used in commercial applications, as presented in Abdelnour (2001); Morse (2001); Slat (2014); Brambini et al. (2017); Lo (1996); Wahl (1992) can benefit from this method in the design process, using a numerical model to test the boom in extreme operating conditions.

8. Conclusions

This paper presented a numerical method to estimate forces in a log boom line by comparing numerical and experimental approaches for hydrodynamic load and motion, considering the rigid-body FSI. The method simulates only one log boom module using CFD tools with the periodic boundary condition to reproduce the fluid flow acting in a single part of the line. The heave and pitch behavior of the log boom structure were compared numerically and experimentally for several Froude number conditions and the most critical side-slip angle, showing good agreement and endorsing the numerical modeling. The CFD load results were implemented in a catenary-like model to calculate forces acting at the ends of a log boom line. On the two proposed scenarios for log boom line geometries, in a Froude number range, the estimate of forces showed a substantial similarity between experimental and numerical techniques.

With proper care previously discussed, these results endorse the viability of applying the developed methods for other Santo Antônio's log boom lines, allowing the study in actual operating conditions, with hundreds of modules connected. One can also study extreme conditions with high loads on the log boom lines, helping the hydropower plant staff organize preventive maintenance to avoid structural damage. The method can aid the design of new modules, especially when it requires the complex numerical modeling presented here. Although it is usually presented in low-velocity flow, applications involving debris containment for trash management can also benefit from the work made here.

Acknowledgments

The authors would like to thank Gustavo de Goes Gomes for the help with the CFD simulations, the technicians and researchers of the Energy Infrastructure Laboratory, and the Santo Antônio Energia for funding the project through the Research and Development fund (PD-06683-0116/2016) of Brazilian Electricity Regulatory Agency (in

Portuguese, Agência Nacional de Energia Elétrica, ANEEL). The first and second authors thank the Fundação de Apoio ao Instituto de Pesquisas Tecnológicas (FIPT), and the last author thanks the Brazilian Innovation Agency (FINEP), under grant number 01.18.0082.01.

References

Abdelnour, R., 2001. Ice Booms in Rivers ; Lessons Learned and the Development of Reliable Solutions Ice Booms Main Characteristics The Wakefield Ice Boom. 11th Workshop on River Ice , 1–10URL: http://cripe.ca/docs/proceedings/11/Abdelnour-2001.pdf.

Bak Khoshnevis, A., Mamouri, A., Mir, F., 2015. An investigation of reynolds number effect on the aerodynamics of bluff body with sharp edges. ADMT Journal 8, –. URL: http://admt.iaumajlesi.ac.ir/article_534934.html.

Brambini, R., Dommergues, B., Maral, H., Sainte-Rose, B., 2017. Hydrodynamics and capture efficiency of plastic cleanup booms: Part i — experiments and dynamic analysis, in: Volume 1: Offshore Technology, American Society of Mechanical Engineers. doi:10.1115/omae2017-61950.

Castro, F.S., Katsuno, E.T., Kogishi, A.M., Paz de Souza, J.M., Dantas, J.L.D.D., 2017a. Structural Analysis for a Reduced Scale Model of a Hydropower Plant Debris Containment Grid, in: Procceedings of the 24th ABCM International Congress of Mechanical Engineering, ABCM, Curitiba. URL: http://abcm.org.br/anais-de-eventos/COB17/0578, doi:10.26678/ABCM.COBEM2017.COB17-0578.

Castro, F.S.d., 2021. Experimental study of the dynamic behavior of a log boom employed at hydropower plants. Master's thesis. University of Sao Paulo. doi:10.11606/d.3.2021.tde-01072021-140939.

Castro, F.S.D., Katsuno, E.T., Dantas, J.L.D., 2017b. Instrumentation Methodology for a Log Containment Grid Model in Towing Tank Tests, in: The 30th American Towing Tank Conference. doi:10.5957/attc-2017-0044.

Choi, J., Yoon, S.B., 2009. Numerical simulations using momentum source wave-maker applied to RANS equation model. Coastal Engineering 56, 1043–1060. doi:10.1016/j.coastaleng.2009.06.009.

Chreim, J.R., Dantas, J.L.D., Lima, A.A.d., 2018. Numerical Analysis of Debris Containment Grid Fluid-Body Interaction, in: Volume 3: Structures, Safety, and Reliability, American Society of Mechanical Engineers. doi:10.1115/OMAE2018-78136.

Chua, K., Eatock Taylor, R., Choo, Y., 2018a. Hydrodynamic interaction of side-by-side floating bodies part I: Development of CFD-based numerical analysis framework and modified potential flow model. Ocean Engineering 166, 404–415. doi:10.1016/j.oceaneng.2017.06.031.

Chua, K., Eatock Taylor, R., Choo, Y., 2018b. Hydrodynamic interaction of side-by-side floating bodies, Part II: Applications of modified linear potential flow and numerical analysis framework to fixed barges. Ocean Engineering 164, 465–481. doi:10.1016/j.oceaneng.2018.06.060.

Girling, B., Lane, T., Benedetti, B., Senta, A.M., Zarma, I.H., Bakken, T.H., Olsson, G., Chavez, F., Rogner, M., 2016. World Energy Resources 2016: Hydropower. Technical Report. World Energy Council. London. URL: https://www.worldenergy.org/wp-content/uploads/2017/03/WEResources_Hydropower_2016.pdf.

Gu, H., Stansby, P., Stallard, T., Carpintero Moreno, E., 2018. Drag, added mass and radiation damping of oscillating vertical cylindrical bodies in heave and surge in still water. Journal of Fluids and Structures 82, 343–356. doi:10.1016/j.jfluidstructs.2018.06.012.

Hassan, A., 2020. Handling river floating debris for dam safety - the state of the practice.

Katsuno, E.T., Castro, F.S.D., Dantas, J.L.D., 2017. Debris Containment Grid CFD validation with Towing Tank Tests, in: The 30th American Towing Tank Conference. doi:10.5957/attc-2017-0043.

Katsuno, E.T., Esteves, F.R., Gomes, G.d.G., Dozzi Dantas, J.L., 2018a. Porous formulation for hydrodynamic simplification of debris containment grid, in: 27 Congresso Internacional de Transporte Aquaviário, Construção Naval e Offshore, Galoa. pp. 23–25. doi:10.17648/sobena-2018-87576.

Katsuno, E.T., Gomes, G.d.G., Castro, F.S.d., Dozzi Dantas, J.L., 2018b. Numerical Analysis of Debris Containment Grid Fluid-Body Interaction, in: Volume 2: CFD and FSI, American Society of Mechanical Engineers. doi:10.1115/OMAE2018-78106.

Leble, V., Barakos, G., 2016. Demonstration of a coupled floating offshore wind turbine analysis with high-fidelity methods. Journal of Fluids and Structures 62, 272–293. doi:10.1016/j.jfluidstructs.2016.02.001.

Liu, Y., Xiao, Q., Incecik, A., Peyrard, C., Wan, D., 2017. Establishing a fully coupled CFD analysis tool for floating offshore wind turbines. Renewable Energy 112, 280–301. doi:10.1016/j.renene.2017.04.052.

Lo, J.M., 1996. Laboratory investigation of single floating booms a and series of booms in the prevention of oil slick and jellyfish movement. Ocean Engineering 23, 519–531. doi:10.1016/0029-8018(95)00064-X.

Løland, G., 1991. Current forces on and flow through fish farms. Phd thesis. Norwegian Institute of Technology. Trondheim.

McQuivey, R.S., 1973. Summary of turbulence data from rivers, conveyance channels, and laboratory flumes: turbulence in water. US Government Printing Office.

Menter, F.R., Kuntz, M., Langtry, R., 2003. Ten Years of Industrial Experience with the SST Turbulence Model Turbulence heat and mass transfer. Turbulence, heat and mass transfer 4, 625–632. URL: http://cfd.mace.manchester.ac.uk/flomania/pds_papers/file_pds-1068134610Menter-SST-paper.pdf.

Morse, B., 2001. Dynamics of ice forces on booms. Cold Regions Science and Technology 33, 29–43. doi:10.1016/S0165-232X(01)00023-4.

Papini, D., 2010. On Shape Control of cables under vertical loads. Master's thesis. Lund University.

Perham, R.E., 1987. Floating debris control: A literature review .

Siemens, 2018. STAR-CCM+ Documentation - version 13.06.

Slat, B., 2014. How the Oceans can Clean Themselves - A Feasibility Study. Technical Report. The Ocean Cleanup. Delft. URL: https://www.theoceancleanup.com/, doi:10.13140/RG.2.2.34283.54566.

Terziev, M., Tezdogan, T., Oguz, E., Gourlay, T., Demirel, Y.K., Incecik, A., 2018. Numerical investigation of the behaviour and performance of ships advancing through restricted shallow waters. Journal of Fluids and Structures 76, 185–215. doi:10.1016/j.jfluidstructs.2017.10.003.

Tran, T.T., Kim, D.H., 2018. A CFD study of coupled aerodynamic-hydrodynamic loads on a semisubmersible floating offshore wind turbine. Wind Energy 21, 70–85. doi:10.1002/we.2145.

Wahl, T.L., 1992. Investigation of Debris and Safety Boom Alternatives for Bureau of Reclamation Use. Technical Report. Bureau of Reclamation - Research and Laboratory Services Division. Denver.

Yu, Y.H., Li, Y., 2013. Reynolds-Averaged Navier–Stokes simulation of the heave performance of a two-body floating-point absorber wave energy system. Computers & Fluids 73, 104–114. doi:10.1016/j.compfluid.2012.10.007.

Ådnanes, H., 2011. Forces on a Net Panel. Master's thesis. Norwegian University of Science and Technology.